Auto-detection of Intermetallic and Eutectic Phases in Microstructure of the AZ91 Mg-alloys by Image Processing Techniques

AZ91 Mg Alaşımlarının Mikroyapısındaki İntermetalik ve Ötektik Fazların Görüntü İşleme Teknikleriyle Otomatik Tespiti

[1]Abdullah ELEN (iD) **, [2]Levent ELEN** (iD)

[1]Bandırma Onyedi Eylül Üniversitesi, Mühendislik ve Doğa Bilimleri Fakültesi, Yazılım Mühendisliği Bölümü, 10200 Bandırma/Balıkesir, Türkiye

[2]Karabük Üniversitesi, T.O.B.B. Teknik Bilimler Meslek Yüksekokulu, Makine ve Metal Teknolojileri Bölümü, 78050 Karabük, Türkiye

[1]aelen@bandirma.edu.tr, [2]leventelen@karabuk.edu.tr

Araştırma Makalesi/Research Article

A B S T R A C T

AZ91, which is used in the production of parts in the aerospace, defense and automotive industries, can be enhanced by the addition of an alloying element or the cooling rate, due to the weak strength and formability properties of advanced technology Mg-alloys. In this study, an image processing-based model is proposed that automatically recognizes the intermetallic and eutectic phases required for the analysis of microstructural properties in AZ91 Mg-alloys. The proposed method consists of two stages; In the first step, the eutectic phase template is obtained as a binary image. In the second step, the binary image containing the intermetallic and eutectic phases is obtained and the result image with only the intermetallic phases is obtained by taking the difference of these two patterns. According to segmentation results of images used in the experimental study, it was calculated as 12% eutectic, 6% intermetallic and 82% alpha phase.

Ö Z E T

Havacılık, savunma ve otomotiv endüstrilerinde parça üretiminde kullanılan AZ91, ileri teknoloji Mg alaşımlarının zayıf mukavemet ve şekillendirilebilirlik özelliklerinden dolayı bir alaşım elementi ilavesi veya soğutma hızı ile geliştirilebilir. Bu çalışmada, AZ91 Mg alaşımlarında mikroyapı özelliklerinin analizi için gerekli olan intermetalik ve ötektik fazları otomatik olarak tanımayı sağlayan görüntü işleme tabanlı bir model önerilmiştir. Önerilen yöntem iki aşamadan meydana gelmektedir; ilk aşamada ikili görüntü olarak ötektik faz şablonu elde edilir. İkinci aşamada ise intermetalik ve ötektik fazları içeren ikili görüntü elde edilir ve bu iki şablonun farkı alınarak yalnızca intermetalik fazların olduğu sonuç görüntüsüne ulaşılır. Deneysel çalışmada kullanılan görüntülerin segmentasyon sonucuna göre ortalama %12 ötektik, %6 intermetalik ve %82 alfa fazı olarak hesaplanmıştır.

ORCID ID: [1]0000-0003-1644-0476
[2]0000-0001-8740-7900

1. INTRODUCTION

Magnesium (Mg) and its alloys, which are the lightest metallic building materials, are extensively used in a variety of engineering fields such as telecommunications, automobile industries, aviation and portable microelectronics due to their low densities as well as their properties like high specific strength, specific hardness, and machinability [1]. In particular, AZ91 alloy containing (on average) Mg–9%Al 0.8%Zn and 0.2%Mn is the most preferred Mg alloy, used in approximately 90% of all Mg casting products [2]. All these sectors, which are among the AZ91 alloys that are increasing in usage day by day, are waiting for AZ91 alloys with more advanced mechanical properties. Therefore, the improvement of the mechanical properties of all Mg-alloys, especially AZ91, has been the focus of academic studies. There have been some studies on improving the mechanical properties of AZ91 alloys by alloying. Elen, in his study, reported that the mechanical properties of Sb and Bi elements added at different rates in the AZ91 alloy improved [3]. Candan et al., in their studies, found that the Ti element increases the mechanical properties (tensile stress up to 18% and yield stress up to 47%) [4]. In his study, Türen reported that the Ultimate tensile strength (UTS) and yield strength (YS) values of the alloy increased with the addition of Sn to AZ91 [5]. In addition, it has been proven by studies [3, 6–8] that in general, Mg-alloys exhibit different mechanical properties with the change of cooling rate. It has been reported in studies [3, 6, 8] that the effect of cooling rate is very important in the development of microstructure and mechanical properties of AZ91 alloys. The changes in the microstructure of the differences in the proportional change of the cooling rate can be clearly observed. These changes in the microstructure have a significant (positive or negative) effect on the mechanical properties of the material. Therefore, the influence of the material's microstructure must be considered in the creation of new manufacturing processes as well as in the existing design and production of materials with high-value components. To quantify each of the microstructures with different properties, it usually requires different analysis procedures [9]. Different techniques are available to measure some microstructural properties of materials. However, the limitations of these techniques need to be developed and reviewed. The American Society for Testing and Materials, short for ASTM, produces industrially accepted standards for microstructural analysis. One of these standards, ASTM E112, defines aerodynamic methods for manually measuring average grain size based on linear intersections of line segments [10]. Parallel lines are drawn on the microstructure image obtained with the optical microscope and the places where they cross the grain boundaries are marked. The average displacement between the marked locations gives the approximate average grain size of the material. Typically, only a subset of the particles is measured and 300 measurements are required to obtain a statistically valid result. The line set can be placed randomly so that the result to be obtained can be free from possible errors. However, the aspect ratio of the grains cannot be calculated in this case. For this reason, the lines are selected manually to be able to measure the width and length of each grain and provide a more detailed measurement. However, users may make mistakes in the determination of the particles to be measured. The ASTM E562 standard, which describes techniques for measuring volume fraction, works based on the point count principle. In line with this standard, a series of dots are placed along the microstructure image, and then an expert indicates which spots are found at each stage. The percentage of points marked at any stage gives the proportion of volume that stage has. The application criteria of these standards create labor and work intensity. The E562 standard requires an estimated 15 minutes' measurement time per image for an experienced user [11]. This slows analysts down and makes them inefficient. These methods are also prone to human error and poor reproducibility, as defining the location of grain boundaries is generally dependent on personal perspective. Such situations make it difficult to detect small microstructural changes and may mislead researchers and researchers in new manufacturing processes or microstructural improvement [9].

Existing approaches to image segmentation can be subdivided depending on the type of algorithms, as well as the types of mathematical convolution applied, artificial intelligence or nature inspired. Such algorithms such as statistical approaches, clustering, artificial neural networks, nonlinear diffusion analysis, and content-based analysis [12] are used not only in the analysis of two-dimensional (2D) images, but also in one-dimensional (1D) signals and three-dimensional (3D) image processing. and plays a very important role in multidimensional calculations. However, as the size of the data increases, so does their complexity. In the case of microstructure photo analysis these methods may be more or less successful [13]. Therefore, the main objective of this study is to examine the structural change kinetic characterization and spatial variation of the α-Mg main matrix phase and β-Mg$_{17}$Al$_{12}$ intermetallic phase in the microstructure of AZ91. For this reason, in this study, the results of changes in any microstructure of AZ91 Mg alloys are analyzed by minimizing user intervention with the image processing method, thus eliminating and/or minimizing the margin of error.

This study was carried out in four stages; In the first stage, some basic concepts related to AZ91 and Mg were emphasized. In the second stage, the preparation process of AZ91 samples used in experimental studies as material and detailed explanations of the proposed method with sample images are given. In the third stage, the percentage ratios of α-Mg, β-Mg$_{17}$Al$_{12}$ (intermetallic) and α-Mg+β-Mg$_{17}$Al$_{12}$ (eutectic) phases in the alloy on the sample microstructure images were automatically determined through experimental studies. At the last stage, the results obtained in the study are summarized.

2. MATERIALS AND METHOD

In this section, automatic segmentation of intermetallic (β-$Mg_{17}Al_{12}$) and eutectic (α-Mg + β-$Mg_{17}Al_{12}$) phases in AZ91 Mg-alloys microstructure images by image processing techniques, calculation of the ratio of these phases in the alloy and GUI developed as a desktop application are discussed.

2.1. The AZ91 Mg-alloys

In the preparation of AZ91 alloy, 99.8% pure Mg and Al were used. The melting process was carried out in an environment closed to the outside atmosphere. The atmosphere of the melting furnace was kept under control by using Argon gas as the shielding gas. After the melting was completed, the melt was poured into a permanent mold made of AISI 1040 quality steel, which was heated to 250°C before casting, in order to prevent possible errors that may arise from the sudden cooling rate.

For metallographic analysis, the surfaces of the samples were polished with 400, 600 and 800 mesh abrasives, using distilled water, and polished using 1μm alumina paste. Then, the surface of the samples was washed with distilled water and alcohol and dried. According to ASTM E407–99 samples were etched with 75% ethylene glycol, 24% distilled water, 1% HNO3 solution. Microstructural observations of the samples were performed using optical and scanning electron microscope (SEM). Microanalysis and determination of the crystal structure of the phases in the studied alloys were performed by X-ray Diffraction (XRD) and Energy-dispersive X-ray Spectroscopy (EDX), respectively. By XRD analysis, the presence of α-Mg phase as well as β-$Mg_{17}Al_{12}$ intermetallic phase was detected in the microstructure of the AZ91 alloy as shown in Fig. (1). In addition to α-Mg matrix, β-$Mg_{17}Al_{12}$ intermetallic as a thin phase at grain boundaries and α-β eutectic has been detected in AZ91 alloy, and this has been reported in different studies [8, 9].
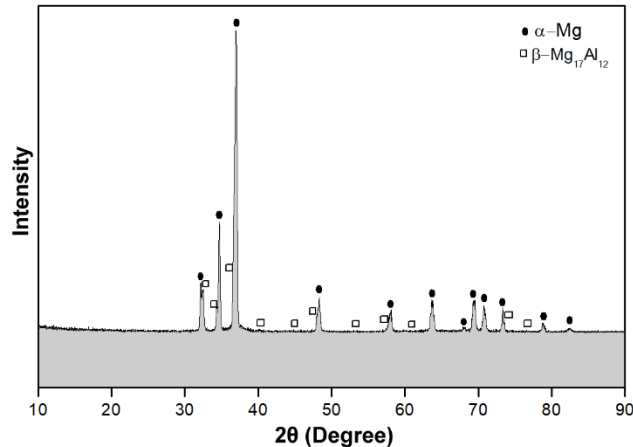

Fig. 1. The X-ray diffraction (XRD) analysis of the AZ91 Mg-alloy.

In addition, EDS analysis was performed for the determination of the phases and the presence of α-Mg, β-$Mg_{17}Al_{12}$ and α-β phases were determined. As seen in Fig. (2), it has been determined that the AZ91 microstructure is generally composed of α-Mg main matrix and consists of eutectic (α+β) and intermetallic β-$Mg_{17}Al_{12}$ phases extending along the grain boundaries.
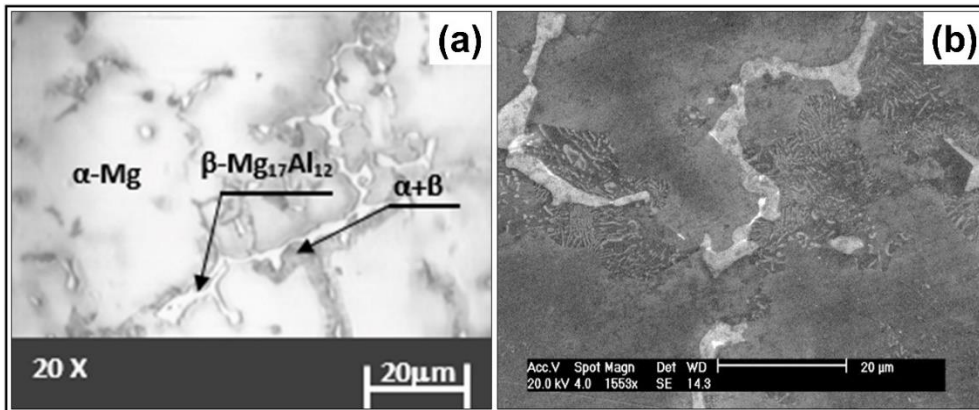

Fig. 2. Microstructure images of the AZ91 Mg-alloy in section A after casting; (a) optical microscope, (b) Scanning Electron Microscope (SEM).

SEM images and EDX analysis of AZ91 are given in Fig. (3). When the SEM images were examined, the particles dispersed on the main matrix phase were detected. As a result of the EDX analysis, they were found to be rich in Al and Mg content.
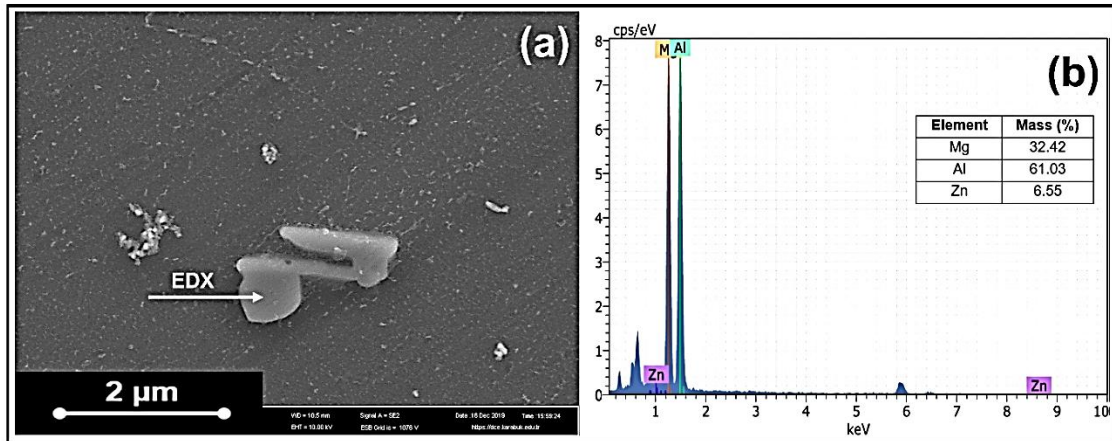

Fig. 3. Alloy of AZ91 (a) SEM image and EDX analysis.

2.2. Proposed Method

The proposed method provides automatic segmentation of eutectic and intermetallic phases in microstructure images of AZ91 alloys. This process is carried out in two stages. In the first step, pixel areas representing the eutectic phases in the microstructure image are detected. In the second step, the input image is preprocessed for the segmentation of the intermetallic phases, and then the pixel regions representing the intermetallic phases are found by subtracting the eutectic phase image obtained in the first step. The flow chart of the proposed method is shown in Fig. (4).
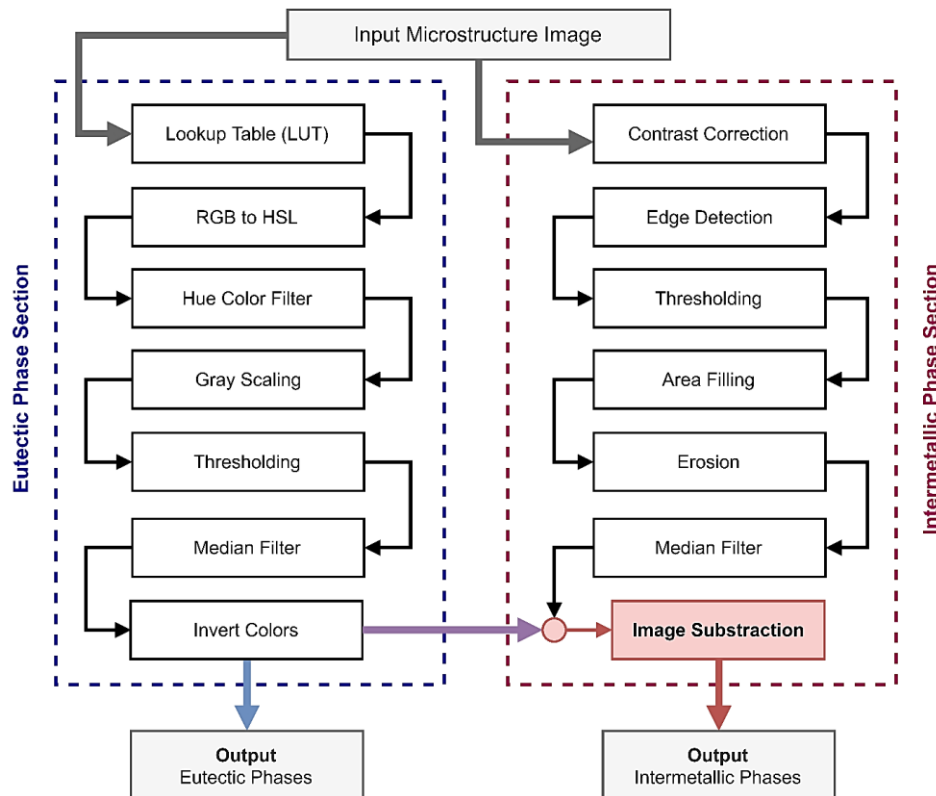

Fig. 4. Flowchart of the proposed method.

Lookup Table (LUT) is a method that enables coloring operations to express images with high color depth in simpler colors or to highlight desired objects in grayscale images. The LUT performs these operations using a reference table called a color map or palette [14], which generates the output value for each pixel in the image as shown in Eq. (1). In this study, "Union Jack" lookup table (See Appendix-1) was used.

$$LUT = \{\{0, [R_{out}, G_{out}, B_{out}]\}, ..., \{255, [R_{out}, G_{out}, B_{out}]\}\}; \tag{1}$$

In the first step of the proposed method, the eutectic phases of the AZ91 alloy in the microstructure images obtained in grayscale were highlighted. Thus, the pixel values containing the eutectic phases in the input image are highlighted in blue, which can be easily distinguished from the others, as shown in Fig. (5).
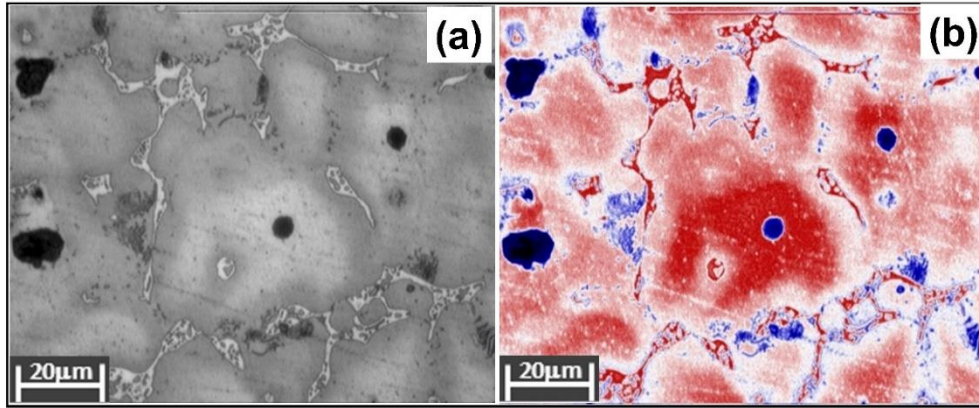

Fig. 5. Applying LUT to the input image; (a) input image, (b) output image.

In the next step, it is converted from RGB color space to HSL, as shown in Eq. (2), to isolate the eutectic phases in the output image obtained by the LUT.

$$Cmax = \max(R/255, G/255, B/255),$$
$$Cmin = \min(R/255, G/255, B/255),$$
$$\Delta = Cmax - Cmin,$$
$$L = (Cmax + Cmin)/2,$$
$$H = \begin{cases} 0°, & \Delta = 0 \\ 60° \times \left(0 + \dfrac{G/255 - B/255}{\Delta}\right), & Cmax = R/255 \\ 60° \times \left(2 + \dfrac{B/255 - R/255}{\Delta}\right), & Cmax = G/255 \\ 60° \times \left(4 + \dfrac{R/255 - G/255}{\Delta}\right), & Cmax = B/255 \end{cases} \tag{2}$$
$$S = \begin{cases} 0, & \Delta = 0 \\ \dfrac{\Delta}{1 - |2L - 1|}, & otherwise \end{cases}$$

Then, it was determined that the eutectic phase intervals in the image are between 180 and 300 degrees according to the Hue component of the HSL color space shown in Fig. (6), and a Hue filter function was developed accordingly, as shown in Algorithm 1. Thus, all pixel areas other than the eutectic phases are painted white, removing unnecessary details on the image.
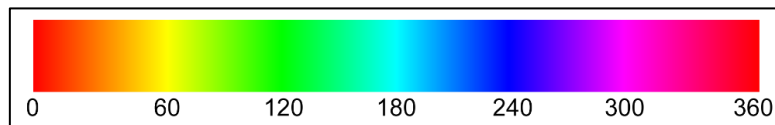

**Fig. 6.** Hue component in the HSL encodings of the RGB color-space.

Algorithm 1. Applying the Hue filter to image.

```
 1:  function ApplyHueFilter(Image img)
 2:      imgHSL ← ConvertToHSL(img);
 3:      for i ← 0 to img.Width do
 4:          for j ← 0 to img.Height do
 5:              set Hue ← imgHSL.GetHue(i, j);
 6:              set WhiteColor ← new Color(255, 255, 255);
 7:              if (Hue < 180 and Hue >300)
 8:                  img.SetPixel(i, j, WhiteColor);
 9:              end if
10:          end for
11:      end for
12:      return img;
13:  end function
```


The image obtained as a result of applying the Hue color filter is shown in Fig. (7).
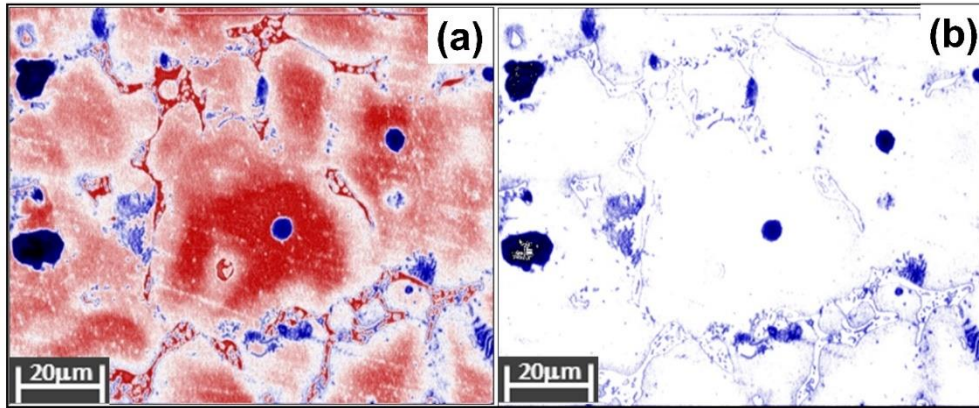
Fig. 7. Applying Hue color filter; (a) input image, (b) output image.

Up to this stage, the eutectic phases in the microstructure images have been segmented to a large extent. In the next and subsequent stages, the image colors are inverted in the final processing step by applying gray scaling, the Otsu thresholding and Median filtering to reduce the effect of pixels representing intermetallic phases in the image and to segment intermetallic phases. Pixels representing intermetallic phases in microstructure images are closer to the background color spectrum than eutectic phases. Therefore, as the first processing step, the contrast correction of the microstructure images taken with the microscope as shown in Fig. (8), and then the enhancement of the border regions with the Kirsch [15] edge detection algorithm was provided.
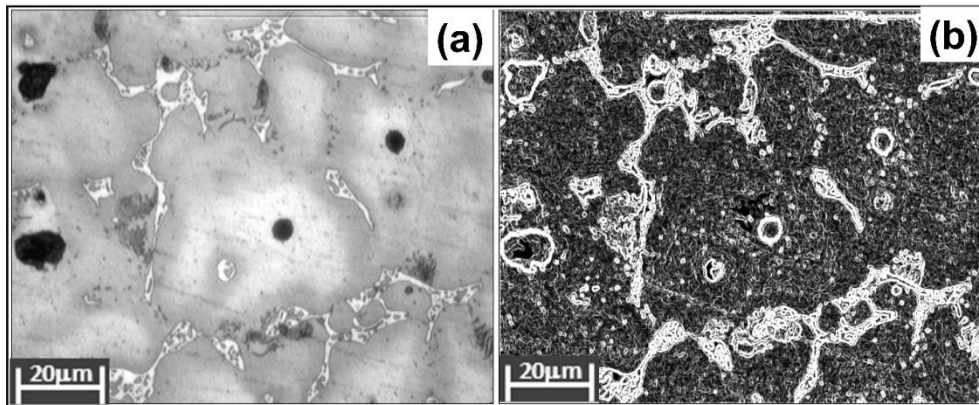
Fig. 8. Contrast correction and edge detection; (a) contrast-corrected input image, (b) Kirsch edge detection result.

In the next step, the edge-detected gray-scale image was converted to binary format with Huang [16] thresholding method as shown in Fig. (9), and Hole Filling (HF) method was applied to prevent possible information loss in pixels representing intermetallic phases.

The HF consists of two stages; firstly, the objects in the binary image are detected by the method of Connected Components Labeling (CCL). In the CCL method, if we consider that an image represented by R comes from S discrete regions, objects in the image can be calculated as in Eq. (3). In the second stage, each discrete region under a certain size is painted in white color. In this study, we limited the size of the objects to be filled with 50-pixels.

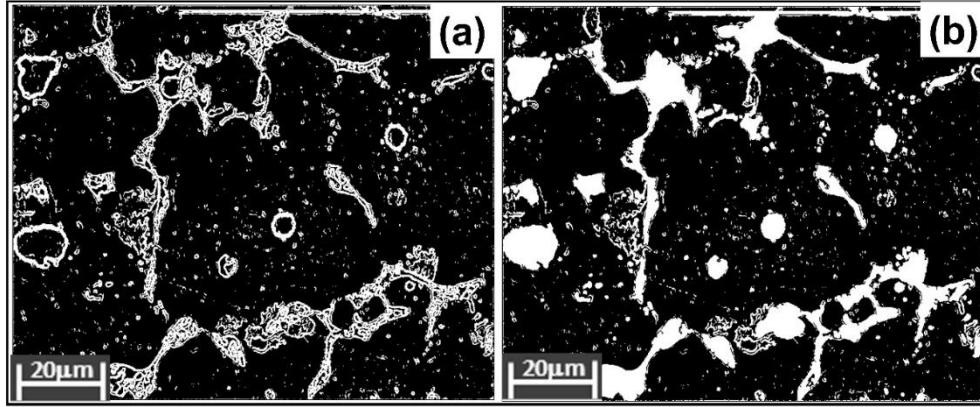$$R_f = R_b^C = \bigcup_{i=1,\ i\neq b}^{S} R_i \tag{3}$$

Fig. 9. Thresholding and area filling; (a) Huang thresholding, (b) hole filling.

Naturally, noise occurs in the images obtained as a result of these processes. In order to overcome these, the erosion method, which is a morphological processing filter, and the Median smoothing filter, respectively, are applied as shown in Fig. (10). It results in some undesired noises in the result image. The Median smoothing filter is applied to remove this problem with Eq. (4).

$$R[x,y] = \text{median}\{g[p,q]\} \tag{4}$$

where $g[p,q]$ is convolution kernel, p and q are kernel index. In this study, a 3×3 convolution matrix is chosen for performance. However, as a result of these processes, as seen in Fig. 10(b), both eutectic and intermetallic phase fields are intertwined in the output image obtained. In the last step, with the image subtraction function given in Algorithm 2, the eutectic phase areas in the output image will be deleted so that only intermetallic phase areas exist.
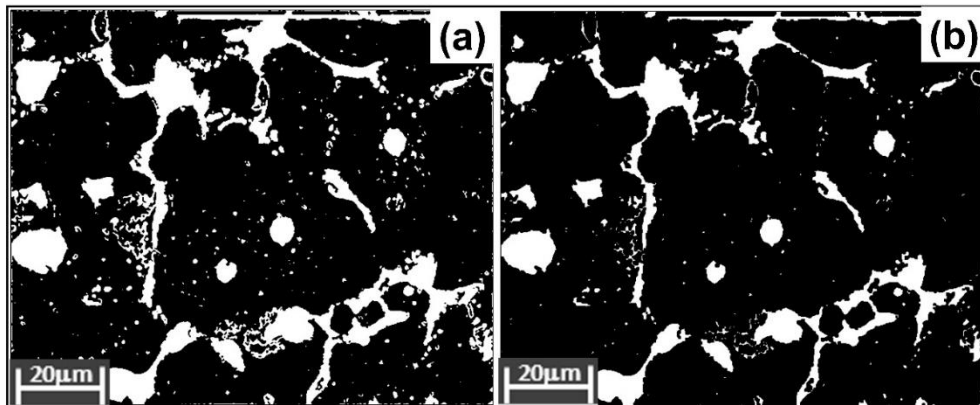

Fig. 10. Applying morphological and smoothing filters; (a) erosion filter, (b) median filter.

Algorithm 2. The function of image subtraction.

```
 1:  function ImageSubtraction(Image imgSource, Image imgTarget)
 2:    set imgResult ← new Image(imgSource.Width, imgSource.Height);
 3:    for i ← 0 to imgSource.Width do
 4:      for j ← 0 to imgSource.Height do
 5:        set pixelSource ← imgSource.GetPixel(i, j);
 6:        set pixelTarget ← imgTarget.GetPixel(i, j);
 7:        if (pixelSource – pixelTarget < 0)
 8:          imgResult.SetPixel(i, j, new Color(0, 0, 0));
 9:        else
10:          set valPixel ← (pixelSource – pixelTarget);
11:          set subColor ← new Color(valPixel, valPixel, valPixel));
12:          imgResult.SetPixel(i, j, subColor);
13:        end if
14:      end for
15:    end for
16:    return imgResult;
17:  end function
```

As can be seen in Fig. (11), the result image in which the intermetallic phases are clearly determined with the image extraction function given in Algorithm 2 is obtained as in Fig. 11(c).
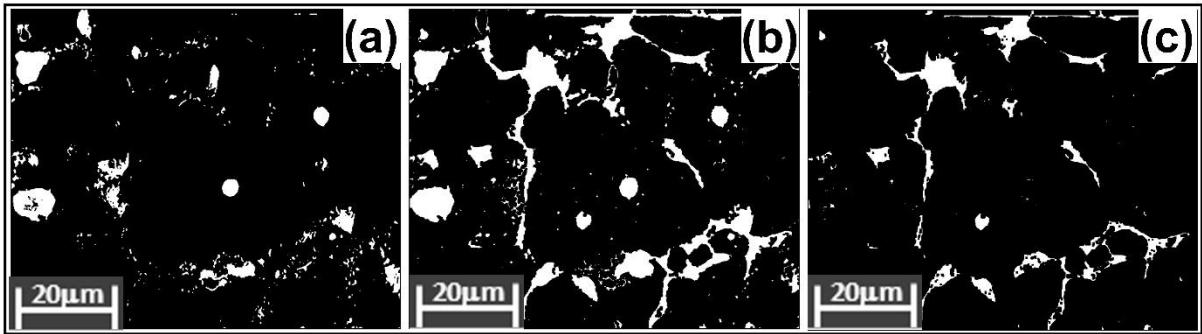
Fig. 11. Image subtraction; a) the extracted eutectic phases, b) the case where the eutectic and intermetallic phases are intertwined, c) the extracted intermetallic phases.

As a result of all these processing steps, the obtained intermetallic and eutectic phase regions applied to the input image using red and blue colors are shown in Fig. (12).
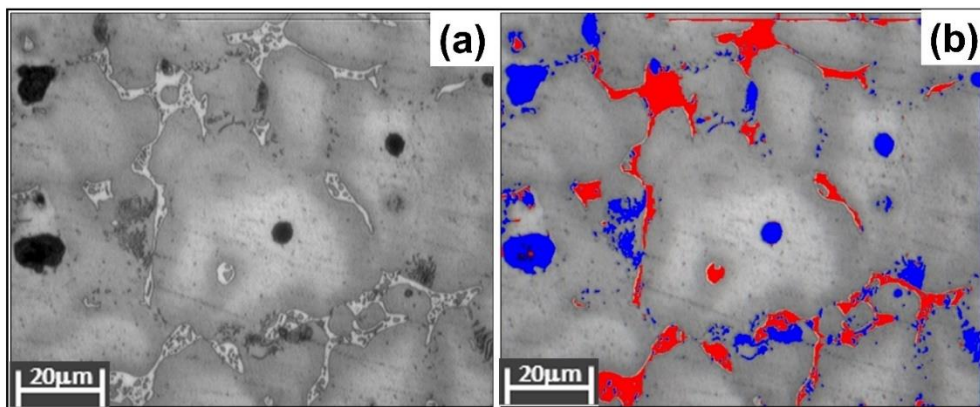
Fig. 12. Automated phase segmentation; (a) input image, (b) output image.

The graphical user interface (GUI) we have developed with the C# programming language is shown in Fig. (13). The numbers shown here are as follows; The region numbered 1 is where the microstructure input image is displayed. Region numbered 2 is where the output image of the microstructure segmented according to the proposed method is shown. The region numbered 3 is the graphical representation of the segmented α, β and α+β

254

phases. The region numbered 4 is where the features of the microstructure input image are displayed. The region numbered 5 is where the intermetallic and eutectic phases are shown separately according to the segmentation result. Finally, in the area numbered 6, there is the control panel of the GUI.
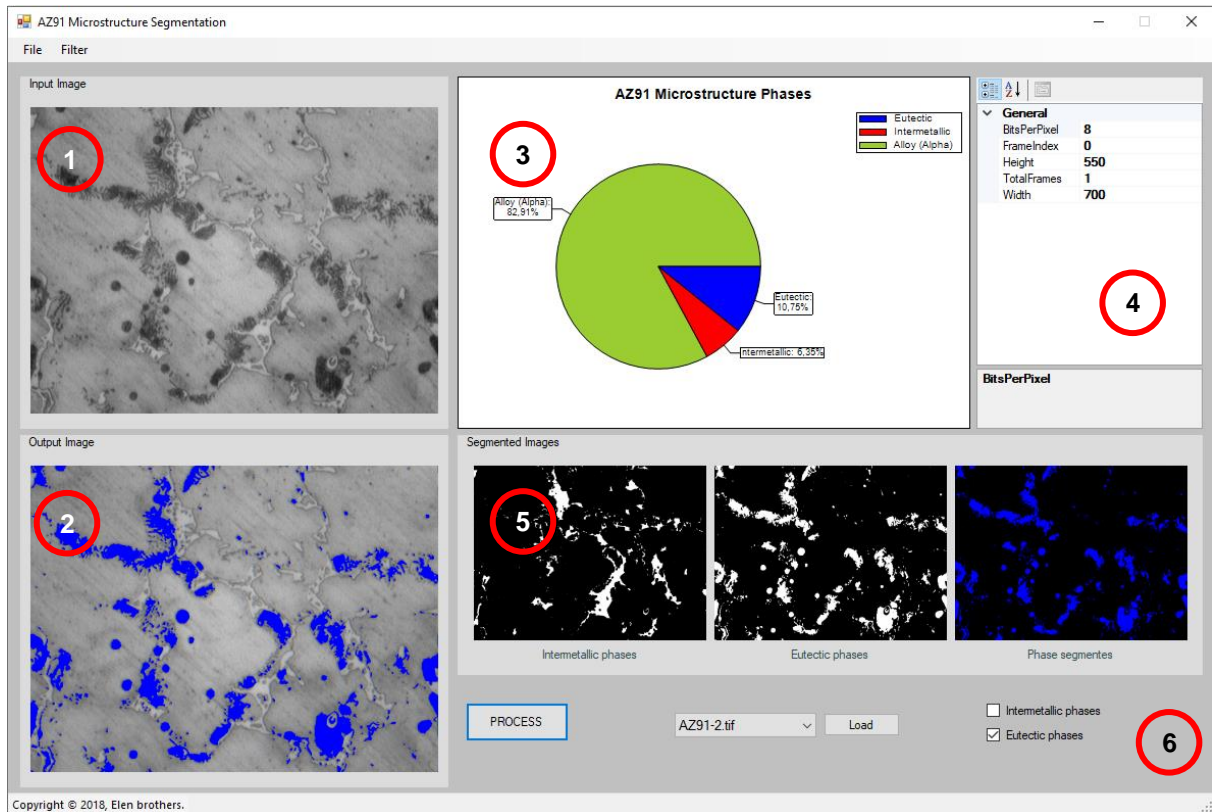

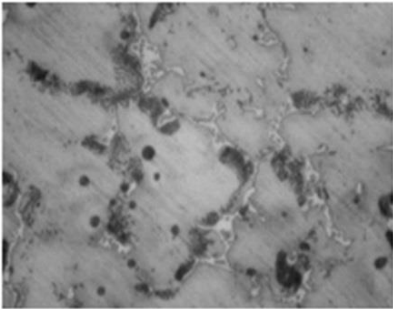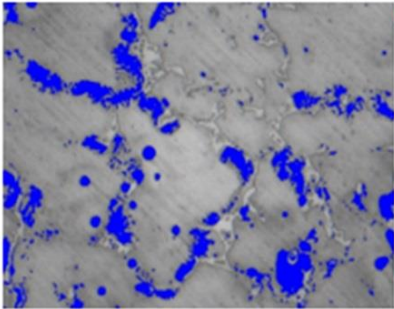**Fig. 13.** The graphical user interface (GUI).
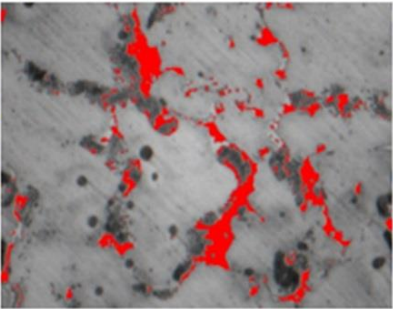
3. EXPERIMENTAL RESULTS

There are 10 different AZ91 microstructure images obtained with optical microscope in experimental studies. These images belong to the samples we prepared in the casting laboratories of Karabük University Metallurgical and Materials Engineering department. Each of the images is monochrome with 700x550 pixel dimensions and was obtained with a 20X microscope objective. With the GUI we have developed, the phases in the microstructure images are automatically detected in less than 500 milliseconds. The measurements we obtained according to the sample dataset as a result of the experimental studies are shown in detail in Table 1.

Table 1. Phase measurement results on the sample dataset.

Sample ID	Phases			Elapsed time (millisecond)
	Eutectic	**Intermetallic**	**Alpha**	
AZ91-01	5,54%	5,59%	88,87%	477
AZ91-02	10,74%	6,35%	82,91%	493
AZ91-03	15,46%	6,33%	78,21%	496
AZ91-04	19,05%	5,72%	75,23%	462
AZ91-05	14,12%	3,82%	82,06%	447
AZ91-06	10,66%	6,74%	82,60%	446
AZ91-07	10,60%	5,27%	84,13%	467
AZ91-08	14,23%	8,30%	77,47%	451
AZ91-09	10,37%	3,31%	86,32%	452
AZ91-10	11,31%	4,30%	84,40%	474

Table 2 shows the segmented phase results of some microstructure images in the sample dataset.

Table 2. Phase segmentation results on the sample dataset.

	Segmentation Results	
Input image	**Eutectic phases**	**Intermetallic phases**
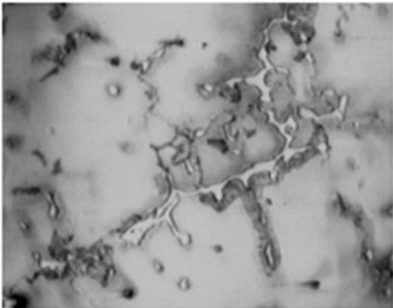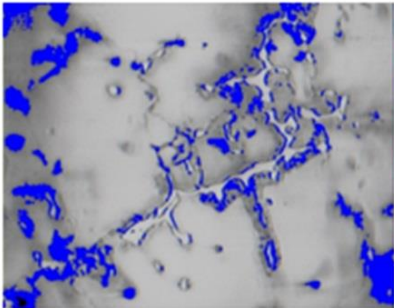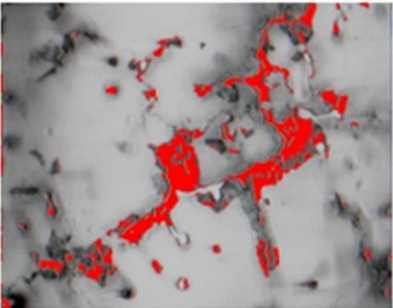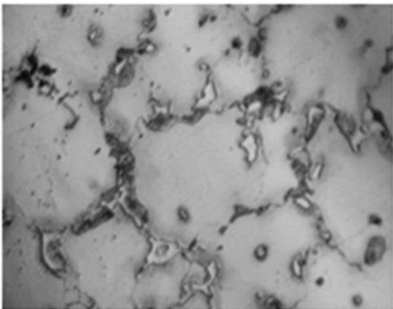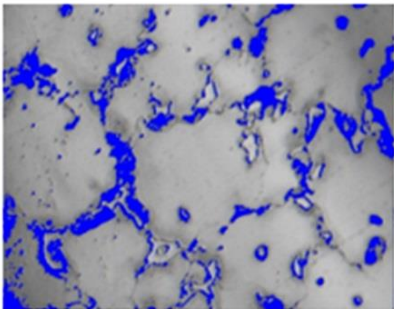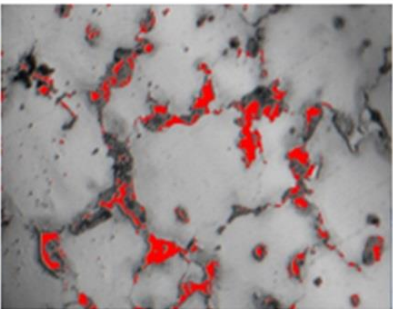
4. CONCLUSION

The microstructure of AZ91 Mg alloys, which we used in our experimental studies, was observed to consist of α-Mg and aluminum-rich β-$Mg_{17}Al_{12}$ intermetallic phases in general. However, the presence of α+β-eutectic phases was detected near the grain boundaries. In order to quantitatively characterize these phases detected in the microstructure of AZ91, an automatic image analysis model was developed and successfully applied. In addition, this application does not apply to AZ91 alloy, which does not contain any other element and does only under normal cooling conditions. At the same time, besides cooling rate, it is valid for artificial or natural aging etc. Because the ratios/types of phases are changes with increasing time because of aging [17]. Therefore, it is a method applicable to different types of alloys and alloys with aging and cooling rates. Because this method is a type of software that includes variation of complex mathematical expressions such as surface analysis, areal size calculation and proportional distributions of phases from simple 2D optical microscope images. With the image processing method, the detection and quantification of complex phases such as eutectic phase with very small deviations and high accuracy has become a fast and easy process. However, the deformation processes applied to the alloys (*forging, rolling, extrusion, etc.*), the addition of different alloying elements or the cooling rate, make it easier to overcome the difficulties of determining the volumetric amount of intermetallic and main matrix phases by making them thinner. Possible deviations that may arise as a result of the analysis are due to the fact that the micro-voids resulting from the acid etching process performed before the microstructure imaging are burned excessively due to acid penetration or that the particles left by the abrasives while applying the surface treatment (*sanding and polishing*) are perceived as phases as a result of sticking to the surface. However, it has been determined that these deviations, which may occur in samples with a clean surface treatment, are in an acceptable range. Since automatic analysis of AZ91 Mg-alloys microstructure properties by image processing methods has not been studied before, the proposed method is promising for new studies in this field. As a result of this study, it is thought that the developed model and the results obtained will shed light on similar studies by adding important information to the literature.

Author Contributions

Each author contributed equally to the study.

Conflict of interest

The authors declare that there is no conflict of interest between them.

REFERENCES

[1] L. Gaines, R. Cuenca, S. Wu, and F. Stodolsky, "Potential automotive uses of wrought magnesium alloys", Argonne National Lab., IL (United States), ANL/ES/CP-89958; CONF-9604136-21, 1996.

[2] C. Blawert, N. Hort, and K. U. Kainer, "Automotive Applications of Magnesium and Its Alloys", Trans. Indian Inst. Met., vol. 57, no. 4, p. 12, 2004.

[3] L. Elen, "Effects of Bi and Sb Additions with Solidification Rate on The Microstructure and Mechanical Properties of The AZ91 Alloys", M.Sc. Thesis, Karabük University, Graduate School of Natural and Applied Sciences Department of Metal Education, 2012.

[4] S. Candan, M. Ünal, E. Koç, Y. Türen, and E. Candan, "Effects of Titanium Addition on Mechanical and Corrosion Behaviours of AZ91 Magnesium Alloy", Journal of Alloys and Compounds, vol. 509, no. 5, pp. 1958-1963, 2011.

[5] Y. Türen, "Effect of Sn Addition on Microstructure, Mechanical and Casting Properties of AZ91 Alloy", Materials and Design, vol. 49, pp. 1009-1015, 2013.

[6] L. Elen, Y. Türen, and E. Koç, "Effects of Solidification Rate on Microstructure and Mechanical Properties with Sb at Different Ratio of AZ91 Quality Mg Alloy", International Journal of Engineering Research and Development, vol. 11, no. 2, pp. 451-463, 2019.

[7] L. Elen, B. Çiçek, E. Koç, Y. Türen, Y. Sun, and H. Ahlatcı, "Effects of Alloying Element and Cooling Rate on Properties of AM60 Mg Alloy", Mater. Res. Express, vol. 6, no. 9, pp. 096511, 2019.

[8] M. Ünal, "Effects of Solidification Rate and Sb Additions on Microstructure and Mechanical Properties of As Cast AM60 Magnesium Alloys", International Journal of Cast Metals Research, vol. 27, no. 2, pp. 80–86, 2014.

[9] A. Campbell, P. Murray, E. Yakushina, S. Marshall, and W. Ion, "New Methods for Automatic Quantification of Microstructural Features Using Digital Image Processing," Materials and Design, vol. 141, pp. 395-406, 2018.

[10] ASTM E112, "Test Methods for Determining Average Grain Size," ASTM International.

[11] ASTM E562, "ASTM E562: Standard Test Method for Determining Volume Fraction by Systematic Manual Point Count."

[12] A. Elen, and M. K. Turan, "A new approach for fully automated segmentation of peripheral blood smears", International Journal of Advanced and Applied Sciences, vol. 5, no. 1, pp. 81-93, 2018.

[13] L. Rauch, and L. Madej, "Application of the Automatic Image Processing in Modeling of the Deformation Mechanisms Based on the Digital Representation of Microstructure", International Journal for Multiscale Computational Engineering, vol. 8, no. 3, pp. 343–356, 2010.

[14] R. Bourne, "Fundamentals of digital imaging in medicine", Springer Science and Business Media, pp. 20-21, 2010.

[15] R. Kirsch, "Computer determination of the constituent structure of biological images", Computers and Biomedical Research, vol. 4, no. 3, pp. 315-328, 1971.

[16] L.-K. Huang, and M.-J. J. Wang, "Image thresholding by minimizing the measures of fuzziness", Pattern Recognition, vol. 28, no. 1, pp. 41–51, 1995.

[17] B. Çiçek, T. Aydoğmuş and Y. Sun, "A basic study on artificial aging in Mg-10Al$_{12}$Si+1Pb alloy", Materials Research Express, vol. 7, no. 1, pp. 1-9, 2020.

APPENDIX-1: Lookup table: "Union Jack"

#	RGB	#	RGB	#	RGB	#	RGB	#	RGB	#	RGB	#	RGB	#	RGB
0	(0, 0, 0)	32	(0, 0, 95)	64	(0, 0, 190)	96	(127, 127, 222)	128	(255, 255, 255)	160	(222, 127, 127)	192	(190, 0, 0)	224	(222, 127, 127)
1	(0, 0, 2)	33	(0, 0, 97)	65	(3, 3, 191)	97	(131, 131, 223)	129	(253, 251, 251)	161	(221, 123, 123)	193	(191, 3, 3)	225	(223, 131, 131)
2	(0, 0, 5)	34	(0, 0, 100)	66	(7, 7, 192)	98	(135, 135, 224)	130	(252, 247, 247)	162	(220, 119, 119)	194	(192, 7, 7)	226	(224, 135, 135)
3	(0, 0, 8)	35	(0, 0, 103)	67	(11, 11, 193)	99	(139, 139, 225)	131	(251, 243, 243)	163	(219, 115, 115)	195	(193, 11, 11)	227	(225, 139, 139)
4	(0, 0, 11)	36	(0, 0, 106)	68	(15, 15, 194)	100	(143, 143, 226)	132	(250, 239, 239)	164	(218, 111, 111)	196	(194, 15, 15)	228	(226, 143, 143)
5	(0, 0, 14)	37	(0, 0, 109)	69	(19, 19, 195)	101	(147, 147, 227)	133	(249, 235, 235)	165	(217, 107, 107)	197	(195, 19, 19)	229	(227, 147, 147)
6	(0, 0, 17)	38	(0, 0, 112)	70	(23, 23, 196)	102	(151, 151, 228)	134	(248, 231, 231)	166	(216, 103, 103)	198	(196, 23, 23)	230	(228, 151, 151)
7	(0, 0, 20)	39	(0, 0, 115)	71	(27, 27, 197)	103	(155, 155, 229)	135	(247, 227, 227)	167	(215, 99, 99)	199	(197, 27, 27)	231	(229, 155, 155)
8	(0, 0, 23)	40	(0, 0, 118)	72	(31, 31, 198)	104	(159, 159, 230)	136	(246, 223, 223)	168	(214, 95, 95)	200	(198, 31, 31)	232	(230, 159, 159)
9	(0, 0, 26)	41	(0, 0, 121)	73	(35, 35, 199)	105	(163, 163, 231)	137	(245, 219, 219)	169	(213, 91, 91)	201	(199, 35, 35)	233	(231, 163, 163)
10	(0, 0, 29)	42	(0, 0, 124)	74	(39, 39, 200)	106	(167, 167, 232)	138	(244, 215, 215)	170	(212, 87, 87)	202	(200, 39, 39)	234	(232, 167, 167)
11	(0, 0, 32)	43	(0, 0, 127)	75	(43, 43, 201)	107	(171, 171, 233)	139	(243, 211, 211)	171	(211, 83, 83)	203	(201, 43, 43)	235	(233, 171, 171)
12	(0, 0, 35)	44	(0, 0, 130)	76	(47, 47, 202)	108	(175, 175, 234)	140	(242, 207, 207)	172	(210, 79, 79)	204	(202, 47, 47)	236	(234, 175, 175)
13	(0, 0, 38)	45	(0, 0, 133)	77	(51, 51, 203)	109	(179, 179, 235)	141	(241, 203, 203)	173	(209, 75, 75)	205	(203, 51, 51)	237	(235, 179, 179)
14	(0, 0, 41)	46	(0, 0, 136)	78	(55, 55, 204)	110	(183, 183, 236)	142	(240, 199, 199)	174	(208, 71, 71)	206	(204, 55, 55)	238	(236, 183, 183)
15	(0, 0, 44)	47	(0, 0, 139)	79	(59, 59, 205)	111	(187, 187, 237)	143	(239, 195, 195)	175	(207, 67, 67)	207	(205, 59, 59)	239	(237, 187, 187)
16	(0, 0, 47)	48	(0, 0, 142)	80	(63, 63, 206)	112	(191, 191, 238)	144	(238, 191, 191)	176	(206, 63, 63)	208	(206, 63, 63)	240	(238, 191, 191)
17	(0, 0, 50)	49	(0, 0, 145)	81	(67, 67, 207)	113	(195, 195, 239)	145	(237, 187, 187)	177	(205, 59, 59)	209	(207, 67, 67)	241	(239, 195, 195)
18	(0, 0, 53)	50	(0, 0, 148)	82	(71, 71, 208)	114	(199, 199, 240)	146	(236, 183, 183)	178	(204, 55, 55)	210	(208, 71, 71)	242	(240, 199, 199)
19	(0, 0, 56)	51	(0, 0, 151)	83	(75, 75, 209)	115	(203, 203, 241)	147	(235, 179, 179)	179	(203, 51, 51)	211	(209, 75, 75)	243	(241, 203, 203)
20	(0, 0, 59)	52	(0, 0, 154)	84	(79, 79, 210)	116	(207, 207, 242)	148	(234, 175, 175)	180	(202, 47, 47)	212	(210, 79, 79)	244	(242, 207, 207)
21	(0, 0, 62)	53	(0, 0, 157)	85	(83, 83, 211)	117	(211, 211, 243)	149	(233, 171, 171)	181	(201, 43, 43)	213	(211, 83, 83)	245	(243, 211, 211)
22	(0, 0, 65)	54	(0, 0, 160)	86	(87, 87, 212)	118	(215, 215, 244)	150	(232, 167, 167)	182	(200, 39, 39)	214	(212, 87, 87)	246	(244, 215, 215)
23	(0, 0, 68)	55	(0, 0, 163)	87	(91, 91, 213)	119	(219, 219, 245)	151	(231, 163, 163)	183	(199, 35, 35)	215	(213, 91, 91)	247	(245, 219, 219)
24	(0, 0, 71)	56	(0, 0, 166)	88	(95, 95, 214)	120	(223, 223, 246)	152	(230, 159, 159)	184	(198, 31, 31)	216	(214, 95, 95)	248	(246, 223, 223)
25	(0, 0, 74)	57	(0, 0, 169)	89	(99, 99, 215)	121	(227, 227, 247)	153	(229, 155, 155)	185	(197, 27, 27)	217	(215, 99, 99)	249	(247, 227, 227)
26	(0, 0, 77)	58	(0, 0, 172)	90	(103, 103, 216)	122	(231, 231, 248)	154	(228, 151, 151)	186	(196, 23, 23)	218	(216, 103, 103)	250	(248, 231, 231)
27	(0, 0, 80)	59	(0, 0, 175)	91	(107, 107, 217)	123	(235, 235, 249)	155	(227, 147, 147)	187	(195, 19, 19)	219	(217, 107, 107)	251	(249, 235, 235)
28	(0, 0, 83)	60	(0, 0, 178)	92	(111, 111, 218)	124	(239, 239, 250)	156	(226, 143, 143)	188	(194, 15, 15)	220	(218, 111, 111)	252	(250, 239, 239)
29	(0, 0, 86)	61	(0, 0, 181)	93	(115, 115, 219)	125	(243, 243, 251)	157	(225, 139, 139)	189	(193, 11, 11)	221	(219, 115, 115)	253	(251, 243, 243)
30	(0, 0, 89)	62	(0, 0, 184)	94	(119, 119, 220)	126	(247, 247, 252)	158	(224, 135, 135)	190	(192, 7, 7)	222	(220, 119, 119)	254	(252, 247, 247)
31	(0, 0, 92)	63	(0, 0, 190)	95	(123, 123, 221)	127	(255, 255, 255)	159	(223, 131, 131)	191	(190, 0, 0)	223	(221, 123, 123)	255	(255, 255, 255)